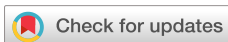


RESEARCH ARTICLE | JULY 01 2024

Chemical heterogeneity size effects at nanoscale on interface thermal resistance of solid–liquid polymer interface via molecular dynamics simulations

Qing-Yao Luo ; Donatas Surblys ; Hiroki Matsubara ; Taku Ohara 

AIP Advances 14, 075305 (2024)

<https://doi.org/10.1063/5.0218506>

Articles You May Be Interested In

Surface wettability of silicon nanopillar array structures fabricated by biotemplate ultimate top-down processes

J. Vac. Sci. Technol. A (February 2021)

Sliding-friction-dependent stress at the graphene/LiNbO₃ interface around the critical temperature of the stress-free state

AIP Advances (February 2019)

Dynamic changes in network synchrony reveal resting-state functional networks

Chaos (February 2015)

08 January 2025 05:02:17

AIP Advances

Why Publish With Us?



19 DAYS
average time
to 1st decision



500+ VIEWS
per article (average)



INCLUSIVE
scope

[Learn More](#)




Chemical heterogeneity size effects at nanoscale on interface thermal resistance of solid–liquid polymer interface via molecular dynamics simulations

Cite as: AIP Advances 14, 075305 (2024); doi: 10.1063/5.0218506

Submitted: 11 May 2024 • Accepted: 12 June 2024 •

Published Online: 1 July 2024



View Online



Export Citation



CrossMark

Qing-Yao Luo,^{1,2,a)}  Donatas Surblys,¹  Hiroki Matsubara,¹  and Taku Ohara¹ 

AFFILIATIONS

¹Institute of Fluid Science, Tohoku University, Sendai, Japan

²Department of Finemechanics, Graduate School of Engineering, Tohoku University, Sendai, Japan

^{a)}Author to whom correspondence should be addressed: luo.qingyao.s8@dc.tohoku.ac.jp

ABSTRACT

The shrinking size of integrated chips poses thermal management challenges. Understanding the size effect of chemical heterogeneity on solid–liquid interfacial thermal transfer is essential for heterogeneous chip design, yet the underlying mechanisms remain lacking. The present work used the liquid *n*-alkanes as the thermal interface material between solid platinum substrates. To characterize chemical heterogeneity, periodic solid surface patterns composed of patches with alternating solid–liquid affinities were constructed. By using non-equilibrium molecular dynamics simulations, we investigated the size effect of chemically heterogeneous patterns on interfacial thermal resistance (ITR) at the nanoscale. At larger heterogeneity sizes, i.e., larger patch sizes, most alkane molecules directly in contact weak interaction patches cannot interact with strong interaction patches due to long atomic distances. In the case of alkanes in contact a cold substrate, alkanes in contact weak interaction patches transferred thermal energy to the substrate at a lower rate than those in contact strong interaction patches. The different rates resulted in the higher temperature of alkanes in contact weak interaction patches than those in contact strong interaction patches and, therefore, a larger disparity between temperature jump at the strong interaction areas and that at the weak interaction areas. The non-uniformity of temperature jump distribution increased ITR when compared to the heterogeneous surface system characterized by a smaller patch size with a more uniform temperature distribution in the plane perpendicular to the heat flux direction. In addition, the classical parallel thermal resistance model predicted ITR accurately for the heterogeneous surface systems with small size patches but overestimated overall thermal resistance.

© 2024 Author(s). All article content, except where otherwise noted, is licensed under a Creative Commons Attribution-NonCommercial-NoDerivs 4.0 International (CC BY-NC-ND) license (<https://creativecommons.org/licenses/by-nc-nd/4.0/>). <https://doi.org/10.1063/5.0218506>

I. INTRODUCTION

High-density circuit integration is one of the primary trends in semiconductor chips. Effective thermal management of chips is essential to maintaining this tendency. To mitigate the thermal resistance caused by air in heat transfer between the chip and heat sink, thermal interface materials (TIMs) are often used in the industry, usually in liquid or adhesive forms, and are applied directly between these components. However, the interfacial thermal resistance (ITR) still exists at two solid–TIM interfaces because of differences in

electronic and vibrational properties.¹ Moreover, as semiconductor process nodes have approached the angstrom-scale,^{2,3} the ITR at solid–TIM interfaces is becoming a significant obstacle to chip thermal management, attributed to the high rate of heat dissipation.⁴ Therefore, understanding the solid–liquid interfacial heat transfer at the atomic level is imperative to enable further development in semiconductor design and thermal management.

Although the semiconductor manufacturing process has achieved very small sizes, further dimension reduction has slowed down due to physical and technological limitations. As an alternative

path to further advance semiconductor performance and efficiency, the industry is shifting its focus to stacking dies into one chip, such as the techniques of system on chip and system in package.⁵ Integrated dies differ in their intrinsic physical and chemical properties due to their different materials and temperatures resulting from distinct power consumption levels. In addition, the chip surface can also be fabricated with textured patterns⁶ or modified through the addition of surfactants⁷ to regulate interfacial thermal transport. Differences in either the geometric or chemical properties of the multi-chip module will result in a chemically heterogeneous surface.^{8,9} In certain specialized cases, such as in high-performance computing applications or advanced thermal management systems, the dies are not encapsulated with resins but are directly in contact with the TIM, thereby establishing a chemically heterogeneous solid-liquid interface. Because thermal management is essential for efficient chip packaging design, it is necessary to comprehensively understand the chemical heterogeneity effect on the interfacial thermal transport of solid-liquid interfaces, to provide a fundamental theoretical basis.

In molecular dynamics (MD) simulations, chemically heterogeneous surfaces are usually represented by alternating one-dimensional stripes or creating two-dimensional grids. Such stripes or grids have different interfacial affinities.^{10,11} The chemical heterogeneity size, adjusted by the size of the stripes or grid, is an essential parameter of heterogeneous interfaces. The chemical heterogeneity size effect of substrate surfaces on droplet wetting behavior has been extensively studied from a nanoscale perspective. Ritchie *et al.*¹² performed MD simulations of water droplets on a chemically heterogeneous graphite surface. They found that the contact angle of the droplets is only determined by the interfacial affinity at the vicinity of the contact line. Both Zhang *et al.*¹³ and Wang and Wu¹⁴ confirmed this finding, and the latter works uncovered that a smaller heterogeneity size leads to a lower pinning force and a smaller contact angle. In contrast, the size effect of chemical heterogeneity on micro-/nanoscale interfacial heat transfer has received limited attention. To the best of our knowledge, only two groups have conducted relevant research. Gao *et al.*¹⁵ performed MD simulations to elucidate the influence of chemical heterogeneity on water boiling heat transfer on copper surfaces. They produce chemically heterogeneous surfaces by placing grid patterns with varying wettability on the substrate. They observed that a larger proportion of hydrophilic area would reduce the ITR and improve the boiling heat transfer. However, they did not investigate further by varying the stripes and grid patterns sizes. Wei *et al.*¹⁶ used equilibrium MD simulations to study the effect of geometric heterogeneity on the ITR of Au-(*n*-alkanes) systems, where self-assembled monolayers (SAMs) with varying chain lengths were grafted on the interface. In addition to the geometrically heterogeneous surfaces, they considered one chemically heterogeneous surface, which was mostly geometrically uniform by using SH-(CH₂)₅-COOH and SH-(CH₂)₅-CH₃ SAM configurations. Although the aforementioned research has demonstrated that chemical heterogeneity has a concrete effect on ITR, the effective size and related size effects remain unclear. Therefore, the objective of this work is to investigate and clarify chemical heterogeneity and its size effect on ITR at solid-liquid interfaces.

Non-equilibrium molecular dynamics (NEMD) simulations have been proven to be a powerful tool to obtain interfacial thermal

properties, such as ITR.^{17,18} In our previous work, we used platinum substrates with convex and concave surfaces and *n*-alkanes as the liquid TIMs to explore the effect of geometric heterogeneity and molecular sizes of TIMs on the solid-liquid ITR.¹⁹ In the present work, NEMD simulations of chemically heterogeneous Pt-(*n*-alkanes) interfaces are performed. We aim to investigate the size effects of chemical heterogeneity at the nanoscale on the ITR of solid-liquid interfaces and analyze the underlying mechanism. We will also discuss how chemical heterogeneity affects overall thermal resistance (OTR). Two distinct molecular sizes of linear alkanes are utilized to validate the size effect. This is done while considering the relative sizes of heterogeneous surface patterns and sizes of liquid molecules. Finally, the ITR and OTR of chemically heterogeneous surface systems are predicted using the straightforward electrical resistance analogy model, the corresponding optimized model, and one approximation model via equivalent homogeneous interfaces.

II. METHODS

A. Potential models

This work utilized a system consisting of two fcc platinum crystals with (001) face on the surface and the liquid *n*-alkanes positioned between the solid components. The lattice constant of platinum is 3.915 Å. To investigate the effect of the length of linear alkane molecules, octane (C8) and ethane (C2) were used as the liquid. Morse potential was employed to describe the interactions between platinum atoms,²⁰ which reliably reproduces the experimental elastic constants. The force field for each alkane molecule was described by the united-atom NERD potential,²¹ which treats the methylene or methyl group as one single atom. This potential exhibits accuracy in the prediction of transport properties and vapor-liquid equilibrium properties.²²⁻²⁴ The van der Waals (vdW) interactions between platinum and atoms in the alkane molecules were represented by the Lennard-Jones (LJ) potential.

A parameter, η , was introduced to control the affinity between solid and liquid due to vdW interactions, which is a commonly used technique to control the system wettability. The formula for interfacial potential energy between one solid and the liquid is expressed as

$$E_{S-L} = \sum_{i \in S} \sum_{j \in L} \eta_{ij} \phi_{ij}^{LJ} = \sum_{i \in S} \sum_{j \in L} 4\eta_{ij} \epsilon_{S-L} \left[\left(\frac{\sigma_{S-L}}{r_{ij}} \right)^{12} - \left(\frac{\sigma_{S-L}}{r_{ij}} \right)^6 \right], \quad (1)$$

where η_{ij} denotes the affinity between atoms *i* and *j*, which belong to the solid and the liquid, respectively, ϕ^{LJ} denotes the original LJ potential function, σ_{S-L} and ϵ_{S-L} are mixed distance and energy parameters between solid and liquid atoms, respectively, and r_{ij} is the distance between atoms *i* and *j*. Values of $\eta = 0.1$ and $\eta = 0.5$ correspond to hydrophobic and hydrophilic solid-liquid interfacial affinities. To verify the relation between η values and wettability, contact angles of alkane droplets on the solid surface were roughly estimated as described in the [supplementary material](#). At a weak solid-liquid affinity ($\eta = 0.1$), the contact angles of C8 and C2 were 119° and 104°, respectively, while at a strong affinity ($\eta = 0.5$), the contact angles were 57° and 66°, respectively. Therefore, we can

assume that the wettability settings are reasonable and reflect realistic wettability ranges. The average 2D density distribution of the droplets is shown in Fig. S1. In addition, although alkane molecules are hydrophobic in the real world,²⁵ we can still experimentally achieve a heterogeneous Pt-(*n*-alkanes) interface using the techniques such as adding surfactants and grafting -COOH and CH₃ terminated SAMs onto the solid surface.²⁶

The simulation systems were composed of three types of interaction sites, i.e., platinum atoms for the solid surface, and methylene and methyl interaction sites for liquid molecules. The LJ parameters between two sites of different types were obtained by specifying arithmetic and geometric means for the mixed distance and energy parameters, respectively. The cutoff radius of all LJ interactions was set to 12 Å. The specific parameter values of NERD potential of alkane molecules and Morse potential of platinum atoms are listed in Tables SI and SII, respectively.

B. Simulation systems

When referring to the whole system, it is heterogeneous since the system consists of different materials. On the other hand, it is customary to refer to uniform surfaces as “homogeneous” and non-uniform ones as “heterogeneous” in theoretical work concerning interfaces.^{10,27,28} In the chemically heterogeneous surface systems, patches with both weak and strong solid-liquid affinities coexist. As shown in Figs. 1(a) and 1(b), surfaces with heterogeneous stripe-type patches were constructed. Figure 1(c) shows the surface with heterogeneous grid-type patches. For reference, the systems with

stripe- and grid-type patches are labeled as “||” and “#,” respectively, while the preceding number corresponds to the patch width and is explained in Table I.

Ueki *et al.* elaborated that groove edges in geometrically heterogeneous surface systems influence interfacial properties, such as different local interfacial heat fluxes at the top and bottom groove edges.²⁹ The interfaces between patches with varying affinities can also be considered edges. To better characterize the heterogeneity sizes of heterogeneous surface systems, the terminology “affinity unevenness” in the unit of 1/Å was introduced. It was quantified by the ratio of total edge length to the platinum cross-sectional area. For example, Fig. 1(b) is $30l_x/(l_x l_y)$, where l_x and l_y are the system dimensions in the *x* direction and *y* direction, respectively, the product of l_x and l_y is the cross-sectional area of platinum surface, and 30 is the number of edges. Chemical heterogeneity size is assumed to decrease as affinity unevenness increases.

Table I lists the detailed heterogeneous surface compositions and liquid combinations. The pattern ID is the combination of the dimensionless patch width in half lattice parameter of platinum and the symbol representing the type of patches, which serves to distinguish the systems. For systems using the same alkane, their patterns are sorted by the magnitude of their affinity unevenness in ascending order. In addition, pattern 7.5|| has slightly non-periodic arrangement of patches, as shown in Fig. S2(a), but the effect has been confirmed to be negligible to the conclusions of this work.

The simulations of this work were conducted using the Large-scale Atomic/Molecular Massively Parallel Simulator (LAMMPS) program.³⁰ The integration algorithm was the velocity-Verlet

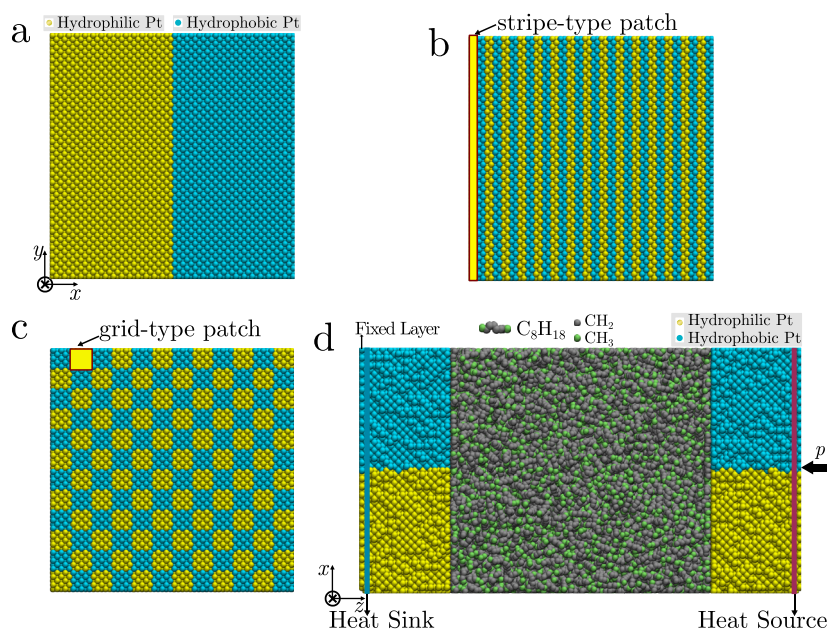


FIG. 1. Illustration of heterogeneous surface compositions and simulation system scheme. Platinum surfaces of patterns 30|| (a) and 2|| (b) with chemical heterogeneity composed of stripe-type patches with altering affinities, in the *x* direction, and surface of pattern 5# (c) with the heterogeneity composed of grid-type patches with altering affinities, in both *x* and *y* directions, where strong interaction patches are colored in yellow and weak interaction ones are colored in cyan; a single strong interaction patch is highlighted by a rectangle with dark red border and yellow fill. (d) Side view of a Pt-C8-Pt system with platinum surface in (a); CH₂ and CH₃ are colored in silver and lime, respectively.

TABLE I. System composition and details of heterogeneous surface patterns.

System	Alkane	Pattern ID	Patch number	Affinity unevenness ($1/\text{\AA}$)	Corresponding figure
1	C8	30	2	0.017	Figure 1(a)
2	C8	15	4	0.034	Figure S2(b)
3	C8	7.5	8	0.068	Figure S2(a)
4	C8	5#	144	0.204	Figure 1(c)
5	C8	2	30	0.255	Figure 1(b)
6	C2	30	2	0.017	Figure 1(a)
7	C2	10	6	0.051	Figure S2(c)
8	C2	5#	144	0.204	Figure 1(c)
9	C2	2	30	0.255	Figure 1(b)

method, with an integration time step length of 1 fs. As an example of the simulation settings, the simulation system of pattern 30||, Pt–C8–Pt system is illustrated in Fig. 1(d). Each of the two solid walls consisted of 22 platinum layers along the direction perpendicular to the solid–liquid interface. Each platinum layer was comprised of 1800 atoms. Heat source and heat sink were installed in the solid walls, and their temperatures were controlled as described later to generate heat flux in the z direction. The walls provided sufficient thickness to ensure phonon relaxation, in accordance with our previous work.³¹ The system dimensions in both the x and y directions were 117.45 Å. It was sufficiently wider than the radius of gyration of C8 chains, ~4.5 Å, evaluated based on the method in Ref. 24. The average length over the last 8 ns of systems in the z direction is provided in Table SIII. The liquid contained 5400 octane or 21 600 ethane molecules with 43 200 interaction sites, CH₃ or CH₂ in the united-atom model, ensuring an adequate thickness of liquid in the heat transfer direction of z to observe the linearity of the temperature gradient within it. The thickness is about 130 Å for C8 and 150 Å for C2. Periodic boundary conditions were applied in the x and y directions, while the z direction was non-periodic.

After initial simulation system construction, annealing was performed by compressing and relaxing the system in the first phase of simulation. The systems were compressed under a high pressure (5 GPa) for 1 ns and relaxed for another 1 ns at 50 and 1 MPa for Pt–C8–Pt and Pt–C2–Pt systems, respectively. The annealing was repeated for five cycles in 10 ns. To adjust the system pressure, the outermost platinum layer on the cold side was fixed, while the platinum layer on the hot side was allowed to move. It was implemented by exerting a constant inward force on the outermost layer of the hot side in the z direction, and the force evenly distributed among the atoms in the layer. In the second phase, the system was equilibrated to reach a steady state. It was determined if a system was fully equilibrated based on the variation of the system heat flux, linearity of temperature distribution in the liquid, and the position evolution of the hot wall. The second phase lasted 40 ns. The last phase was a 64 ns data production simulation. The sampled data were divided into four segments to obtain the standard errors of the mean values of ITR and OTR, while taking statistical inefficiency into account.³² A flow chart of the simulation scheme is provided in Fig. S3. We should note that the solid layer with the heat source was not fixed even after the equilibration phase due to computational resource

constraints. However, this would not have a significant impact on the results of this work.

Throughout the simulation, Langevin thermostats with a damping coefficient of 0.1 ps were applied to the heat sink and heat source installed in the second outermost platinum layers, with different control temperatures for the cold and the hot walls. In order to compare the simulation results of chemically heterogeneous Pt–C8 interface systems with those of previously studied geometrically heterogeneous and homogeneous Pt–C8 interface systems,¹⁹ identical thermodynamic conditions were used. In particular, the heat sink and heat source were set to 480 and 540 K, respectively, and the control pressure was 50 MPa. For C2, which exhibits lower critical constants of density, pressure, and temperature, the temperature range was set to 160 and 220 K, yielding an identical temperature difference of 60 K as in C8. The control pressure of C2 was set one commonly used value of 1 MPa. As the Pt–C8–Pt and Pt–C2–Pt systems are compared separately, the different thermodynamic conditions do not affect the conclusions of this work.

In addition to the previously studied homogeneous Pt–C8 interface systems with solid–liquid affinities of $\eta = 0.1$ and $\eta = 0.5$,¹⁹ four additional homogeneous surface systems were simulated for better comparison with heterogeneous surfaces, in particular, a Pt–C8–Pt system with a solid–liquid affinity of $\eta = 0.3$ and Pt–C2–Pt systems with affinities of $\eta = 0.1$, $\eta = 0.3$, and $\eta = 0.5$. The simulation scheme for the homogeneous surface systems is the same as the heterogeneous surface systems. All the types of homogeneous x – y surfaces are presented in Figs. S2(d)–S2(f).

C. Analysis methods

1. Thermal resistance

Because the hot side of the solid wall is not fixed but oscillates at its equilibrium position, it is somewhat problematic to robustly evaluate the ITR at its solid–liquid interface in this hot side. Only the ITR at the cold side solid–liquid interface is examined in this study. The ITR, R_0 , is calculated by

$$R_0 = \frac{\Delta T_0}{J_z}, \quad (2)$$

where J_z is the average heat flux in the z direction over a period of time, t . J_z is obtained by $J_z = (E_h - E_c)/2At$, where A is the area of

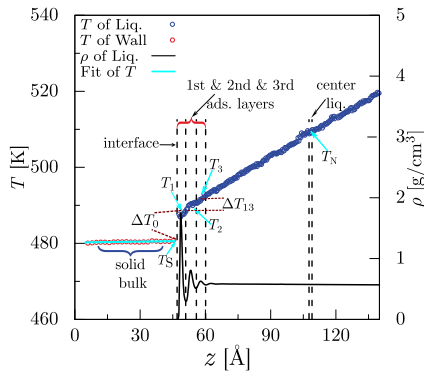


FIG. 2. An illustration of how temperature and density profiles of pattern 5#, Pt-C8-Pt system are used to determine the temperature jumps at the solid-liquid interface, ΔT_0 , and the temperature difference between the average temperature of the i th and j th liquid adsorption layers, ΔT_{ij} . The average temperature of the center of the liquid with a thickness of 2 Å is denoted as T_N , which is used to calculate the temperature difference from that of i th adsorption layer, ΔT_{iN} .

x - y surface and E_h and E_c are the thermal energy input into the heat source and that removed from the heat sink by the Langevin thermostats, respectively, during the period of time, t . ΔT_0 is the temperature jump at the solid-liquid interface.

The density and temperature profiles of pattern 5#, Pt-C8-Pt system are shown in Fig. 2 to elaborate the exact definition of ΔT_0 . The red and blue circles represent the average temperature of the solid and liquid, respectively. The solid was binned into separate solid layers according to platinum lattice, while the liquid had bins of 0.1 Å. The midpoint between the solid layer adjacent to the liquid phase and the first bin with non-zero liquid density was selected as the solid-liquid interface position. The temperature of the bulk solid, consisting of the middle 16 layers, was linearly fitted and extrapolated to determine the solid temperature at the solid-liquid interface, denoted as T_s . For the liquid temperature at the solid-liquid interface, the average temperature of the first liquid adsorption layer instead of the temperature obtained by linear extrapolation was used onto the solid-liquid interface when computing the interfacial temperature jump. We examined that the ITR trends evaluated using the two methods were consistent. However, the average temperature method allowed for the decomposition of the thermal resistance of the liquid into contributions from the liquid adsorption layers and the liquid bulk. This provided a more detailed understanding of the thermal transport mechanism. The liquid adsorption layers were separated by density dips, as indicated by the black dashed lines in Fig. 2. The average temperature of the first liquid adsorption layer denoted as T_1 was obtained by averaging the temperatures of liquid bins within this layer based on the equipartition theorem. The temperature jump is then equal to $T_1 - T_s$, indicated by the two dashed dark red lines in Fig. 2.

The OTR generally refers to the thermal resistance of heat flowing from the hot solid-liquid interface to the cold interface. Its calculation can determine if heterogeneity affects the bulk liquid. In this work, to eliminate the influence of hot wall oscillation, the OTR is only considered for the cold half of the system. In particular, the sum of ITR at the cold side solid-liquid interface and the thermal

resistance of half of the liquid adjacent to the heat sink (R_L) is characterized as the OTR (R_t). The thermal resistance of the liquid was further subdivided into contributions from the liquid adsorption layers and the liquid bulk.

To better describe the decomposition schemes of OTR, we begin by presenting the general rule of subscripts chosen for denoting the temperature, temperature differences, and thermal resistance of components in the liquid. As displayed in Fig. 2, the average temperature of the i th liquid adsorption layer is denoted as T_i and that of the bulk liquid center is denoted as T_N . The temperature difference between the average temperature of the i th and j th liquid adsorption layers is denoted as ΔT_{ij} and obtained by $\Delta T_{ij} = T_j - T_i$. Similarly, the temperature difference between the average temperature of the i th liquid adsorption layer and the center of the liquid is denoted as ΔT_{iN} and obtained by $\Delta T_{iN} = T_N - T_i$. Based on the temperature differences, the thermal resistance from the i th liquid adsorption layer to the j th liquid adsorption layer is denoted as R_{ij} and obtained by $R_{ij} = \Delta T_{ij}/J_z$. Likewise, the remaining thermal resistance from the i th liquid adsorption layer to the center of the liquid is denoted as R_{iN} and obtained by $R_{iN} = \Delta T_{iN}/J_z$. The R_L is the same as R_{1N} , $R_{12} + R_{2N}$, and $R_{13} + R_{3N}$.

Then, the decomposition schemes of OTR can be expressed as

$$R_t = R_0 + R_L = R_0 + R_{12} + R_{2N} = R_0 + R_{13} + R_{3N} = \frac{T_N - T_s}{J_z}, \quad (3)$$

where each term of thermal resistance is obtained by dividing the heat flux by corresponding temperature differences, i.e., $R_i = \Delta T_i/J_z$.

2. A high-resolution estimation of temperature jump

The 2D temperature profiles in x - z dimensions for both patterns 30|| and 5# of heterogeneous Pt-C8 interface systems are presented in Figs. 3(a) and 3(b), respectively. The first liquid adsorption layer was indicated by the black rectangle, whose upper and lower boundaries correspond to the positions of liquid density dip and solid-liquid interface, as can be verified in Fig. 2. In addition, the black rectangles are further divided into stripes based on the patch sizes. Platinum has a nearly uniform temperature distribution in both patterns due to its high thermal conductivity. However, in the temperature distribution within the first liquid adsorption layer, a notable difference between the two patches can be observed in Fig. 3(a), corresponding to areas of strong and weak interactions. Conversely, the temperature distribution of the first liquid adsorption layer in pattern 5# is more uniform, as shown in Fig. 3(b). The 2D temperature profiles of the first liquid adsorption layers in x - y dimensions provided in Fig. S4 also illustrate the uniformity discrepancy between the two patterns. Accordingly, temperature uniformity in the first liquid adsorption layer is one of the key effects of the heterogeneity size. Therefore, to quantify this effect, the overall temperature jump at the sub-solid-liquid interfaces directly above the strong interaction patches ($\Delta T_0^{\text{strong}}$) and that directly above the weak interaction patches (ΔT_0^{weak}) were separately evaluated. By analyzing these data, we can better understand the effects of heterogeneity on interfacial thermal transport. In the following, the word “above” refers specifically to “directly above” unless otherwise stated.

To obtain $\Delta T_0^{\text{strong}}$ and ΔT_0^{weak} of systems with stripe- and grid-type patches, the 2D and 3D temperature profiles of liquid were

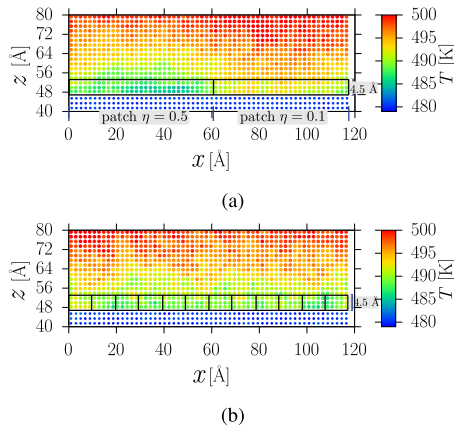


FIG. 3. 2D temperature profiles in x - z dimensions of C8 and platinum near solid-liquid interfaces in patterns 30 (a) and 5 (b). The first liquid adsorption layer with a thickness of 4.5 Å is divided by black lines based on the layout of heterogeneous patches in Figs. 1 (a) and 1(c).

computed via LAMMPS, respectively. In the x direction, the length of sub-2D boxes was set to half of the platinum lattice, and in the z direction, it was 1.5 Å. For the size of sub-3D boxes, to have enough atoms in the statistical box to ensure temperature accuracy, the length in the z direction was set to the same as the thickness of the first liquid adsorption layer. The length in the x and y directions was set to the same as that of one grid-type patch, i.e., 9.8 Å. Using the temperature profiles, the temperature of sub-2D or sub-3D boxes in the first adsorption layer and above the strong interaction patches, denoted as $\bar{T}_1^{\text{strong}}$, was calculated by

$$\bar{T}_1^{\text{strong}} = \frac{\sum_{i=1}^N T_{1i}^{\text{strong}} N_i}{\sum_{i=1}^N N_i}, \quad (4)$$

where T_{1i}^{strong} denotes the temperature of the i th liquid sub-box, which is in the first adsorption layer and above the strong interaction patches, and N_i is the number of liquid atoms in the i th box. Similarly, \bar{T}_1^{weak} can be obtained.

On the other hand, owing to the uniform temperature distribution of platinum, the temperature of solid at the solid-liquid interface determined using the linear extrapolation method, described in Sec. II C 1, is only 0.3–0.6 K higher than the control temperature of the heat sink. For simplicity, both the average temperature of strong interaction patches and weak interaction patches is set to the same value as the temperature of the heat sink, also denoted as T_S , when estimating the two overall temperature jumps. The $\Delta T_0^{\text{strong}}$ and ΔT_0^{weak} are then equal to $\bar{T}_1^{\text{strong}} - T_S$ and $\bar{T}_1^{\text{weak}} - T_S$, respectively. These two values are evaluated every 16 ns and averaged over the last 64 ns to obtain the mean values and corresponding errors, following the method described in Sec. II B for ITR and OTR.

3. Plane heat flux decomposition

Although the total heat flux can be indirectly obtained from Langevin thermostats, directly computing the plane heat flux using atom coordinates, velocities and forces offers deeper insight into the overall mechanism. In this work, specifically, the plane heat flux

at the solid-liquid interface can be decomposed into contributions from the weak and strong solid-liquid interactions.

In the case of the solid-liquid interface, only platinum-methylene and platinum-methyl pairs contribute to heat flux. The formula for heat flux across a plane^{33,34} can be written as

$$J_{z,S-L}A = \frac{1}{2} \sum_{i \in S} \sum_{j \in L} \mathbf{F}_{ij} \cdot (\mathbf{v}_i + \mathbf{v}_j), \quad (5)$$

where \mathbf{F}_{ij} is the force vector between one solid atom i and one liquid atom j and \mathbf{v} is the velocity vector of one atom.

As both strong and weak interaction patches exist in the heterogeneous surface systems, the heat flux can be decomposed into contributions from the weak and strong solid-liquid interactions, respectively. Applying this decomposition to the flux at the solid-liquid interface, the heat flux in Eq. (5) can be expressed as

$$J_{z,S-L} = J_{z,S-L}^{\text{weak}} + J_{z,S-L}^{\text{strong}} = \frac{1}{2A} \sum_{i \in S} \sum_{j \in L} \mathbf{F}_{ij} \cdot (\mathbf{v}_i + \mathbf{v}_j) + \frac{1}{2A} \sum_{k \in S} \sum_{j \in L} \mathbf{F}_{kj} \cdot (\mathbf{v}_k + \mathbf{v}_j), \quad (6)$$

where the subscripts $i \in S^{\text{weak}}$ and $j \in S^{\text{strong}}$ denote the solid atoms with a weak affinity and strong affinity, respectively, and $J_{z,S-L}^{\text{weak}}$ and $J_{z,S-L}^{\text{strong}}$ are the plane heat fluxes contributed by the weak and strong solid-liquid interactions, respectively.

To ensure better accuracy of the plane heat flux calculation, the calculation was conducted after also fixing the wall on the hot side. The sampling time for the Pt-C8-Pt and Pt-C2-Pt systems is 24 and 8 ns, respectively.

4. Modeling OTR and ITR via theoretical formulas and homogeneous surface system

In principle, we can consider that the solid-liquid interface of our heterogeneous surface system is composed of numerous patches connecting the solid and liquid phases in a parallel configuration. At the macroscopic scale, the following parallel formula analogous to electricity can be used to model the thermal resistance of a system from the thermal resistances of its parallel components:^{35,36}

$$\frac{1}{R^{\text{parallel}}} = \sum_{i=1}^n \frac{1}{R_i}, \quad (7)$$

where R^{parallel} is the thermal resistance estimated using the parallel model and R_i is the thermal resistance of each parallel component. In practice, the thermal resistance values for each component can be obtained from separate measurements of equivalent systems, i.e., homogeneous surface systems in our case.

To the extent of our knowledge, no specific model has been verified for the calculation of ITR or OTR of chemically heterogeneous surface systems using the corresponding thermal resistance values of homogeneous surface systems at the nanoscale. Hence, we verify if Eq. (7) models thermal resistances of heterogeneous surface systems at the nanoscale in this work. Heterogeneous surface systems can be considered parallel homogeneous surface systems with solid-liquid affinities of either 0.1 or 0.5. We refer to this model as the parallel model and denote it using the superscript “parallel.” Therefore, in

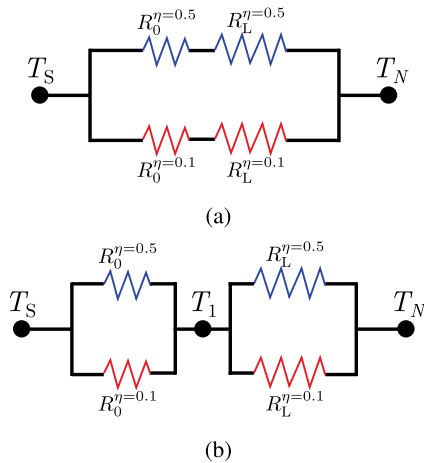


FIG. 4. Schematics of parallel system model (a) and parallel interface model (b), where T_S is the temperature of substrate, T_1 is the average temperature in the first liquid adsorption layer, and T_N is the temperature of liquid at the center position.

accordance with Eq. (7), the ITR of heterogeneous surface systems can be modeled by

$$\frac{1}{R_0^{\text{parallel}}} = \frac{1}{2} \left(\frac{1}{R_0^{\eta=0.1}} + \frac{1}{R_0^{\eta=0.5}} \right), \quad (8)$$

where $R_0^{\eta=0.1}$ and $R_0^{\eta=0.5}$ are the ITR of homogeneous surface systems with solid–liquid affinities of 0.1 and 0.5, respectively. Note that any variable with superscript η is from the homogeneous surface system. The derivation of Eq. (8) assumes that the temperature jump over all patches is uniform, while it is not always the case in reality and will be discussed in Sec. III B 2. In addition, the ITR at the interface above weak and strong interaction patches is assumed to be the same as that of the homogeneous surface systems with $\eta = 0.1$ and $\eta = 0.5$, respectively. In particular, $R_0^{\text{weak}} = R_0^{\eta=0.1}$ and $R_0^{\text{strong}} = R_0^{\eta=0.5}$. It is similar to what is typically assumed at the macroscopic scale, where the thermal resistance of one component in a parallel configuration is the same as the thermal resistance when measuring only the component itself. The $\frac{1}{2}$ reflects that weak or strong interaction

patches occupy half of the interface. A detailed derivation of Eq. (8) is provided in Sec. S1 B.

Likewise, the OTR of heterogeneous surface system can be calculated by

$$\frac{1}{R_t^{\text{P-sys}}} = \frac{1}{2} \left(\frac{1}{R_t^{\eta=0.1}} + \frac{1}{R_t^{\eta=0.5}} \right), \quad (9)$$

where R_t is the sum of ITR and thermal resistance of liquid. In this formula, we assume that all homogeneous surface systems are connected in parallel, as depicted in Fig. 4(a). To distinguish with the following model assuming solid–liquid interfaces and the liquid component are paralleled separately and then connected in series, we refer to this model as the parallel system model and denote it using the superscript “P-sys.”

As will be illustrated in Sec. III C, Eq. (9) is not suitable for modeling the OTR of heterogeneous surface systems. A revised formula is proposed, which is in the form of

$$R_t^{\text{P-iface}} = R_0^{\text{parallel}} + R_L^{\text{parallel}} = R_0^{\text{parallel}} + \frac{2R_L^{\eta=0.1} \cdot R_L^{\eta=0.5}}{R_L^{\eta=0.1} + R_L^{\eta=0.5}}, \quad (10)$$

where R_0^{parallel} is the parallel ITR obtained using Eq. (8) and R_L^{parallel} is the parallel thermal resistance of liquid by applying Eq. (7). In Eq. (10), the heterogeneous surface system is assumed to be constructed by first paralleling the solid–liquid interfaces and the liquid components of homogeneous surface systems separately and then connecting the two parallel components in series, as depicted in Fig. 4(b). Furthermore, as the thermal resistance of the liquid bulk should theoretically be the same for all heterogeneous and homogeneous surface systems, we assume that R_L is the same for these systems. This implies that we assume R_L is not affected by the solid–liquid interface. As a result, this model only parallels the solid–liquid interfaces, and the liquid is considered as a single element connected with the parallel interfaces in series. Hence, we refer to this model as the parallel interface model and denote it using the superscript “P-iface.”

From the existing research, both the experimental measurements³⁷ and NEMD simulations³⁸ demonstrated a quasi-linear relationship between the solid–liquid affinity and interfacial thermal conductance (ITC, inverse of ITR). Given an equal number of strong and weak interaction patches and assuming a linear correlation

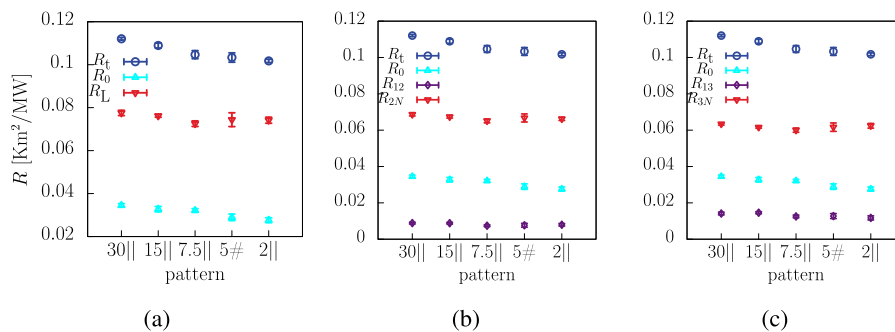


FIG. 5. Decomposition of OTR for C8 liquid systems under different heterogeneity patterns using schemes of $R_t = R_0 + R_L$ (a), $R_t = R_0 + R_{12} + R_{2N}$ (b), and $R_t = R_0 + R_{13} + R_{3N}$ (c).

between affinity and ITC, the ITC of our heterogeneous surface system is expected to approximate that of a homogeneous surface system with an affinity of 0.3 ($\eta = 0.3$), which represents the arithmetic mean of the ITC values from homogeneous surface systems with $\eta = 0.1$ and $\eta = 0.5$. Here, we denote the homogeneous surface system with $\eta = 0.3$ as the homogeneous surface system model with the superscript “ $\eta = 0.3$.” Briefly, we will employ the parallel model and homogeneous surface system model to predict the ITR of heterogeneous surface systems and utilize the parallel system model, parallel interface model, and homogeneous surface system model to predict the OTR.

III. RESULTS AND DISCUSSION

A. Decomposition of OTR

The OTR (R_t) of heterogeneous C8 liquid (Pt–C8–Pt) systems and its components, as illustrated by Eq. (3), are shown in Fig. 5, where the liquid phase resistance is decomposed via two approaches. OTR decreases as the affinity unevenness increases, while it does not change significantly because R_L contributes the most. R_{2N} or R_{3N} , the thermal resistance from the bulk liquid, is almost the same in each pattern. This consistency is expected since the bulk liquid should have identical thermal properties in all of our systems. On the other hand, ITR in Figs. 5(a)–5(c) exhibits similar trends to OTR and so is R_{13} in Fig. 5(c). The similar trends of ITR, R_{13} , and OTR demonstrate that we were able to isolate the effects of ITR and thermal resistance of liquid adsorption layers on OTR. The same tendency can be observed in C2 liquid (Pt–C2–Pt) systems as well, and detailed decomposition results are included in Fig. S5. A conclusion can be drawn that the effects of surface heterogeneity on thermal transfer of SLS systems are localized at the solid–liquid interface, i.e., the effects are mostly on ITR and thermal resistance of adsorption layers. Hence, the main focus will be on ITR when analyzing the heterogeneity size effect in Sec. III B.

Detailed comparisons of the ITR of heterogeneous C8 liquid and C2 liquid systems and its correlation with the heterogeneity size, quantified by the affinity unevenness parameter in Sec. II B, are exhibited in Figs. 6(a) and 6(b), respectively. In Fig. 6(a), the disparity in ITR between patterns 30|| and 2|| is evident and the variation in ITR between patterns 5# and 2|| is relatively minor. In addition,

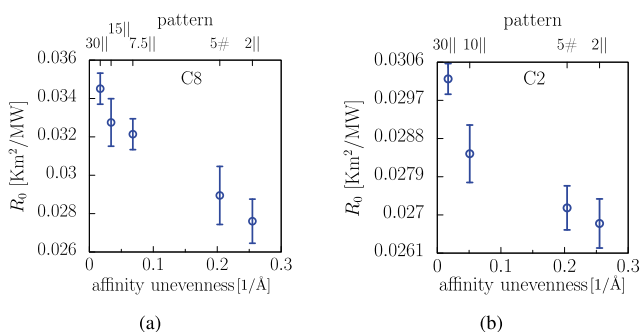


FIG. 6. ITR comparisons among systems under different heterogeneity patterns and the general correlation between ITR and heterogeneity size quantified by affinity unevenness. (a) C8 liquid systems; (b) C2 liquid systems.

TABLE II. Maximum and minimum ITR and OTR among heterogeneous surface systems and comparison with homogeneous surface systems.

Surface uniformity	$R(\text{km}^2/\text{MW})$	Alkane		
		C8	C2	Pattern
Heterogeneous	R_0^{\min}	0.028(1)	0.0270(6)	2
	R_0^{\max}	0.035(1)	0.0300(4)	30
Homogeneous	$R_0^{\eta=0.1}$	0.128(2)	0.1230(6)	$\eta = 0.1$
	$R_0^{\eta=0.5}$	0.016(1)	0.0160(3)	$\eta = 0.5$
Heterogeneous	R_t^{\min}	0.102(1)	0.0800(1)	2
	R_t^{\max}	0.112(1)	0.0860(6)	30
Homogeneous	$R_t^{\eta=0.1}$	0.199(5)	0.1770(4)	$\eta = 0.1$
	$R_t^{\eta=0.5}$	0.090(8)	0.0700(3)	$\eta = 0.5$

Fig. 6(b) shows that the ITR is positively proportional to the heterogeneity size and the sizes of patterns 5# and 2|| are close to each other. Therefore, we can conclude that while the heterogeneity size plays a crucial role, the heterogeneity pattern, no matter in the form of stripe- or grid-type patches, has a limited effect on ITR. On the other hand, somewhat surprisingly, similar trends in C8 liquid and C2 liquid systems indicate that molecular size does not have a dominant effect.

Table II lists the minimum and maximum ITR and OTR of heterogeneous surface systems, whose notations include the superscripts of min and max, respectively. In both C8 liquid and C2 liquid systems, pattern 2|| exhibits the lowest ITR and OTR values. In contrast, pattern 30|| demonstrates the highest ITR and OTR values. The notations of ITR and OTR of homogeneous surface systems with the superscripts of $\eta = 0.1$ or $\eta = 0.5$ denote the solid–liquid affinities of the corresponding homogeneous surface systems. One can find that both ITR and OTR results are within the interval of the corresponding homogeneous surface system values. In particular, thermal transfer is not enhanced beyond what can be obtained with a strong interaction homogeneous surface by introducing chemical heterogeneity. It is consistent with Wei *et al.*¹⁶

B. Analysis of ITR and other interfacial properties

1. Adsorption density and orientation

To better understand the effect of surface heterogeneity, an analysis of structural interface properties was conducted. Previous research demonstrated that the solid–liquid atom pairs within the first coordination shell of solid atoms transfer the major amount of heat across the solid–liquid interface.³⁹ As the number of such solid–liquid atom pairs is directly proportional to the liquid adsorption amount, the liquid adsorption density was evaluated by counting the number of atoms in the first adsorption layer, which is distinguished by the density dips in the liquid density profile as described in Sec. II C 1. As shown in Fig. 7(a), ITR is negatively correlated with liquid adsorption density. The correlation is consistent with our previous work in the case of a weak solid–liquid affinity, where the orientation and the number of liquid adsorption layers are dominant factors in the case of a strong solid–liquid affinity.¹⁹ It indicates an enhancement of thermal transfer at the interface via

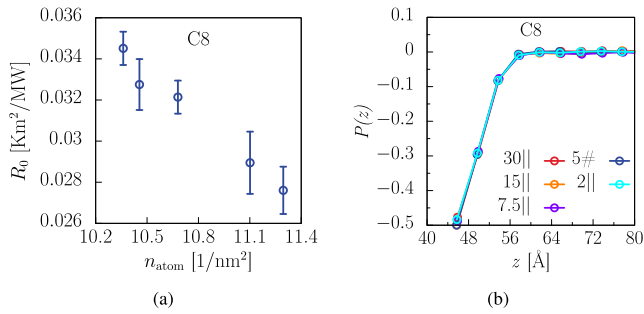


FIG. 7. Structural interfacial properties of heterogeneous C8 liquid systems. (a) Relation between ITR and liquid adsorption density; (b) distribution of orientation order parameter of C8 molecules with respect to the z axis. Structural interfacial properties of heterogeneous C2 liquid systems are added in Fig. S6 since the tendencies are similar to that of heterogeneous C8 liquid systems.

surface adsorption, a phenomenon well-documented in the existing literature.^{38,40}

The orientation of alkane molecules is another key factor that affects interfacial thermal transfer. Lin *et al.*⁴¹ found that a larger fraction of parallel aligned alkyl-pyrene molecules at the graphene-alkanes interface can result in a lower ITR. They attributed the reduction in ITR to the vertically oriented C-H bonds owing to the parallel stacked C-C backbones. The vibration of solidified C-H bonds strengthened phonon transport at the interface. Kawagoe *et al.*⁴² also reported that the cross-plane orientation of linear acrylic acid molecules would decrease the ITR of platinum-polymer interface. In the present work, surface heterogeneity is expected to induce orientation along the heat flux direction in the linear alkane molecules, thereby improving thermal transfer at the interface. As one possible mechanism, we can imagine that strong interaction patches with a limited surface area could force long C8 alkanes to only partially attach to them, leaving dangling tails that would be oriented non-parallel to the solid surface due to repulsive interactions from neighboring weak interaction patches, while the short C2 alkanes would serve as the comparison group.

The scalar order parameter⁴³ was calculated to characterize the orientation of alkane molecules. It is evaluated by the following formula: $P(z) = \frac{1}{2}(3 \cos^2 \theta - 1)$, where θ is the angle between the z axis and the bond connecting one atom and its neighbor-of-neighbor atom in the same alkane molecule, and the angle brackets denote the ensemble average over all these bonds in all molecules. Values range from $P(z) = -0.5$ to $P(z) = 1$, where they correspond to perpendicular and parallel alignment of alkane molecules with respect to the z axis, respectively, and $P(z) = 0$ denotes random orientation. From the distribution of $P(z)$ in Fig. 7(b), one can find that the alkanes in all systems have almost identical orientation profile. In the first liquid adsorption layer, alkanes are perpendicular to the heat flux direction, while being parallel to the solid surface. Therefore, contrary to our initial expectations, surface heterogeneity has little effect on the alkane molecular structure. In addition, it appears that the heterogeneity size effect is independent of molecular size. However, the alkane chains oriented vertical to the x - y surface might be achieved by combining the geometric and chemical roughness and specific functional groups, which will be investigated in the near

future. This insensitivity to alkane molecule length can explain the similar trends for both C8 liquid and C2 liquid observed in Fig. 6.

2. Temperature jump tendencies

As can be seen from the ITR equation in Eq. (2), the temperature jump is a crucial property that determines the ITR. To better observe the effect of heterogeneous surfaces, the temperature jumps at weak and strong solid-liquid interaction areas, ΔT_0^{weak} and $\Delta T_0^{\text{strong}}$, were separately evaluated.

The approach described in Sec. II C 2 was used to obtain Fig. 8. For patterns 5# and 2|| in Fig. 8(a) and patterns 10||, 5#, and 2|| in Fig. 8(b), we observed that the temperature jumps were mostly uniform, with at most 0.5 K difference between T_0^{strong} and T_0^{weak} . The almost identical values between ΔT_0^{weak} and $\Delta T_0^{\text{strong}}$ for these patterns indicate that when the heterogeneity size falls below a certain threshold, the temperature distribution of liquid becomes uniform in the x - y plane. In contrast to the uniform temperature distribution for the cases of patterns 5# and 2||, a distinct difference between ΔT_0^{weak} and $\Delta T_0^{\text{strong}}$ can be found in patterns 30|| and 15|| in Fig. 8(a) and pattern 30|| in Fig. 8(b), with large heterogeneity sizes, implying an uneven temperature distribution in the liquid adsorption layer. One such case of an uneven temperature distribution is clearly illustrated via a 2D temperature profile of the C8 liquid system in pattern 30|| in Fig. 3(a). Such a large discrepancy between ΔT_0^{weak} and $\Delta T_0^{\text{strong}}$ is also possible in real-world systems. One can imagine a macroscopic SLS system where the surface is half plastic and half metal and the liquid is water. In the case of heat flowing from the liquid to the solid, provided a large enough temperature gradient, it is foreseeable that the water temperature adjacent to the metal substrate would be lower than that near the plastic substrate.

Overall, Fig. 8 illustrates that the liquid in systems with large size heterogeneity has an uneven temperature distribution. However, as the heterogeneity size decreases, the liquid temperature distribution becomes more uniform. From the ITR results in Fig. 6, we can find that systems with an uneven temperature distribution have a higher ITR than those with a uniform temperature distribution. The uneven temperature distribution within the first liquid adsorption layer generates a subtle temperature gradient in either

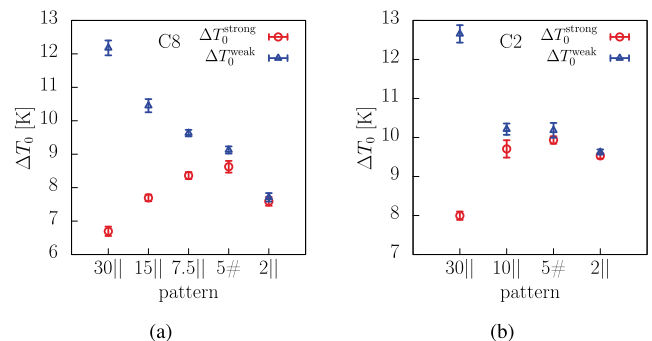


FIG. 8. Temperature jumps at the weak interaction interface (blue) and strong interaction interface (red) for each heterogeneous surface system. (a) C8 liquid systems; (b) C2 liquid systems.

the x or y direction. It is expected to induce the heat flux from the liquid above the weak interaction patches to the liquid above the strong interaction patches and, thus, increase the ITR. However, the computed heat flux in either the x or y direction for both patterns 30|| (uneven temperature) and 5# (even temperature) of C2 liquid systems is small and with much noise, 15–30 MW/m² with 50% error, which makes it difficult to confirm the above speculation. On the other hand, Zhang *et al.* simulated porous alumina systems using the finite element method and demonstrated that the thermal resistance of systems with an uneven temperature distribution is higher than that with a uniform temperature distribution.⁴⁴ Although it cannot be easily compared to this work, it supports the heterogeneity effect.

Moreover, among the patterns with a uniform temperature distribution, the last pattern with the smallest heterogeneity size has the minimum temperature jump and the minimum ITR. It implies that the ITR can be further reduced by decreasing the heterogeneity size even when the liquid temperature distribution becomes uniform. Upon closer examination of Fig. 8, the values of ΔT_0^{weak} and $\Delta T_0^{\text{strong}}$ in pattern 2|| are identical, while a minor disparity between them exists in pattern 5# in Fig. 8(a) and patterns 10|| and 5# in Fig. 8(b). It indicates that the temperature distribution of liquid in the last pattern is uniform at a higher resolution than that in other patterns. A comparison of 2D temperature profiles of the first C8 adsorption layer in the x - y plane between the last two patterns and the corresponding probability distributions of temperature values are provided in Figs. S7(a)–S7(c). The same type of information for C2 liquid systems is provided in Figs. S7(d)–S7(f). According to the probability distribution of C8 liquid and C2 liquid systems, the temperature distribution of liquid in the last pattern is a bit more uniform.

3. Plane heat flux decomposition

Similar to the temperature jump in Sec. III B 2, heat flux essentially determines ITR and provides valuable insight into the heat transfer mechanism. Following Sec. II C 3, the heat flux over the solid–liquid interface was computed and decomposed.

The ratios between the decomposed heat flux due to strong and weak solid–liquid interactions are shown in Figs. 9(a) and 9(b) for C8 and C2 liquid systems, respectively. The actual values of the decomposed heat flux are provided in Fig. S8. An overall trend can be found in both Figs. 9(a) and 9(b) that the ratio decreases as the heterogeneity size diminishes. In general, we notice that despite the contact area of both patches with strong and weak affinities being the same, the patches with a strong affinity majorly contribute to the heat flux. Moreover, the ratio between the contributions from the two types of interactions tends to approach closer as the heterogeneity size decreases.

To get a better physical picture of the heat transfer mechanism, snapshots of solid–liquid interfaces were also provided. As mentioned in Sec. III B 1, liquid atoms in the first coordination shell around the solid atoms, i.e., the first adsorption layer at the solid–liquid interface, are responsible for the majority of heat transfer. The shell size was determined by liquid density dips described in Sec. II C 1. To count the number of liquid atoms in the first adsorption layer as precisely as possible, each pattern used the corresponding accurate shell size, which is in the range of 4.4–4.6 Å. Figures 9(c) and 9(d) depict the liquid C8 molecules in the first

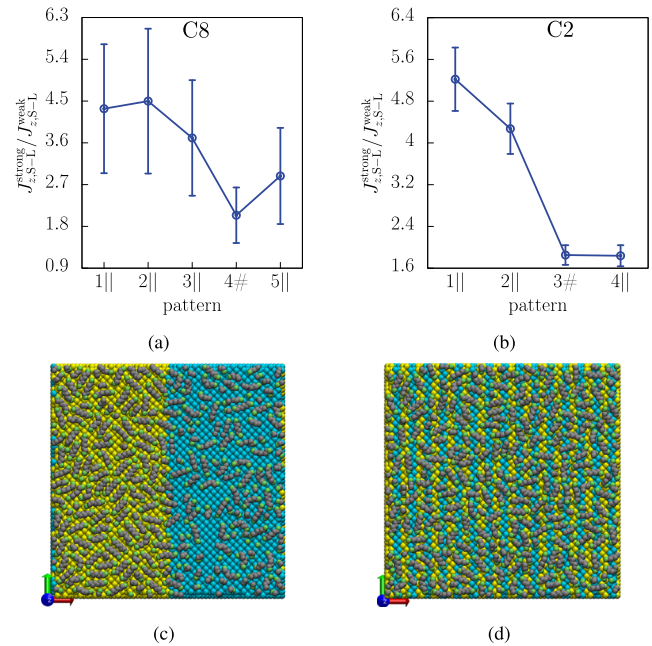


FIG. 9. Ratios between decomposed heat flux due to strong and weak solid–liquid interactions of heterogeneous Pt–C8 (a) and heterogeneous Pt–C2 (b) interface systems. Snapshots of C8 molecules in the first adsorption layer of patterns 30|| (c) and 2|| (d).

adsorption layer of patterns 30|| and 2||, respectively. In Fig. 9(c), fewer liquid atoms were adsorbed on the weak interaction patches of the substrate, which reduced the heat flux via the weak solid–liquid interactions. The disparity in the number of liquid atoms adsorbed on the strong and weak interaction patches was regarded as the main factor resulting in the difference between $J_{z,S-L}^{\text{strong}}$ and $J_{z,S-L}^{\text{weak}}$. On the other hand, the liquid atoms were uniformly distributed on the substrate of pattern 2|| as shown in Fig. 9(d). The length of one patch in the x direction is 3.915 Å, which is smaller than the coordination shell radius. This enables all the liquid atoms in the first adsorption layer to interact with both strong and weak interaction patches. It results in similar magnitudes of $J_{z,S-L}^{\text{strong}}$ and $J_{z,S-L}^{\text{weak}}$ in last two pattern systems of both C8 liquid and C2 liquid systems. Moreover, the strongly interacting solid–liquid pairs transfer more heat than the weakly interacting pairs even though the numbers of the two types of pairs are the same. It is the reason why the ratio values of $J_{z,S-L}^{\text{strong}} / J_{z,S-L}^{\text{weak}}$ are larger than 1.

C. Modeling thermal resistance

Accurately measuring the ITR of nanostructures remains challenging.⁴⁵ If we could identify a model, where inputting the ITR of each patch would reliably reproduce the measured ITR of heterogeneous surface systems, it would provide an approach to estimate the ITR of heterogeneous surface systems based on the priori data obtained from homogeneous surface systems. An identical line of thought can also be applied to modeling OTR, where the thermal resistance of the liquid phase also becomes an additional input to

the model. Based on this idea, the performance of two ITR and three OTR models described in Sec. II C 4 is assessed in this section.

Figures 10(a) and 10(b) present the comparison results among the ITR of heterogeneous surface systems, the parallel model [Eq. (8)] and homogeneous surface system ($\eta = 0.3$) model for C8 liquid and C2 liquid systems, respectively. According to the parallel model described in Sec. II C 4, the size of pattern used in Eq. (8) is not significant. The ITR calculated using Eq. (8) will remain consistent as long as the ratio of the surface area of the $\eta = 0.5$ system to that of the $\eta = 0.1$ system matches the ratio of the surface area of strong interaction patches to weak interaction patches in the heterogeneous surface system. We obtained the local ITR of the strong and weak interaction areas by using the temperature jumps in Fig. 8 and the decomposed plane heat flux in Fig. S8. Based on the local ITR results in Fig. S9, we confirmed the assumption that the ITR of patches is the same as that of homogeneous systems is not correct. The ITR of the parallel model gives a good match with the ITR of heterogeneous surface systems where the temperature distribution is almost uniform, as shown in Fig. 8, i.e., patterns 5# and 2||. In addition, R_0^{parallel} also overlaps with the ITR of pattern 10|| in C2 liquid systems, whose temperature distribution is also not uneven. In other words, the parallel model is only applicable when the temperature jumps are identical for both types of patches. In other cases, the parallel model underestimates the ITR, because the temperature jumps are significantly lower at high affinity patches, resulting in a lower heat flux. Hence, while $R_0^{\text{weak}} = R_0^{\eta=0.1}$ and $R_0^{\text{strong}} = R_0^{\eta=0.5}$ assumptions were not necessary, the uniform distribution of spatial

and energetic properties in the liquid near the solid–liquid interface was crucial for the parallel model to work. This uniformity can be evaluated by examining the deviation between temperature jumps in the strong and weak interaction areas.

The ITC results of homogeneous C8 liquid and C2 liquid systems with η of 0.1, 0.3, and 0.5 are shown in Figs. 10(c) and 10(d), where the gray dashed lines connect the ITC of homogeneous surface systems. The gray dashed lines are straight, verifying the assumption for the homogeneous surface system model in Sec. II C 4 that the ITC of homogeneous surface systems is linearly proportional to the solid–liquid affinity. Based on the linear relation, the ITC of heterogeneous surface systems can be mapped to get the corresponding solid–liquid affinity of homogeneous surface systems. As the vertical gray shadow in Fig. 10(c) covers, the corresponding affinity of homogeneous C8 liquid systems ranges from 2.65 to 3.35. The corresponding affinity of heterogeneous C2 liquid systems ranges from 2.81 to 3.24 as shown in Fig. 10(d). It explains why the ITR of the homogeneous surface system model locates in the range of the ITR of heterogeneous surface systems in Figs. 10(a) and 10(b). We can confirm that periodic chemical heterogeneity using patches with solid–liquid affinities of x and y can produce the similar effect as the homogeneous surface system with a solid–liquid affinity of $(x + y)/2$. However, we cannot determine which heterogeneity pattern the homogeneous surface system model precisely corresponds to.

In addition to the homogeneous surface system model, two types of parallel models, including a parallel system model [Eq. (9)] and a parallel interface model [Eq. (10)], were used to model the OTR of heterogeneous surface systems. As depicted in Fig. 4, the parallel system model assumes connecting homogeneous surface systems in parallel to compose one heterogeneous surface system. In contrast, the parallel interface model assumes connecting only the solid–liquid interfaces of homogeneous surface systems in parallel and then connecting the liquid component with the paralleled interface in series. As the temperature difference in Eq. (3) used to calculate OTR is almost identical for all the systems, the OTR difference among the systems is mainly due to the heat flux difference. As shown in Fig. 11(a), the heat flux values from the Langevin thermostats rather than the local heat flux in Fig. S8(a), of heterogeneous C8 liquid systems increases gradually as the heterogeneity size decreases. The range of flux of all the patterns is from 260 to 280 MW/m². The average of heat flux in homogeneous surface systems with η of 0.1 and 0.5 is 232 MW/m². It is the direct reason that causes the OTR modeled by the parallel system model to be much larger than the actual OTR of heterogeneous surface systems in Fig. 11(b). On the other hand, the heat flux of the homogeneous surface system with η of 0.3 lies in the middle of the range of heat flux of heterogeneous surface systems. This explains why the OTR of the homogeneous surface system model can serve as a reference to roughly estimate the OTR of heterogeneous surface systems. The same thing can be observed in C2 liquid systems in Figs. 11(c) and 11(d). In addition, the heat flux values of C2 liquid systems, obtained from Langevin values, are more consistent with the plane heat flux at the solid–liquid interface compared to those of C8 liquid systems, primarily due to smaller statistical errors.

In the parallel interface model, we assumed identical thermal resistance of the liquid (R_L) for all systems using the same type of alkane. If this assumption holds true, the parallel interface model

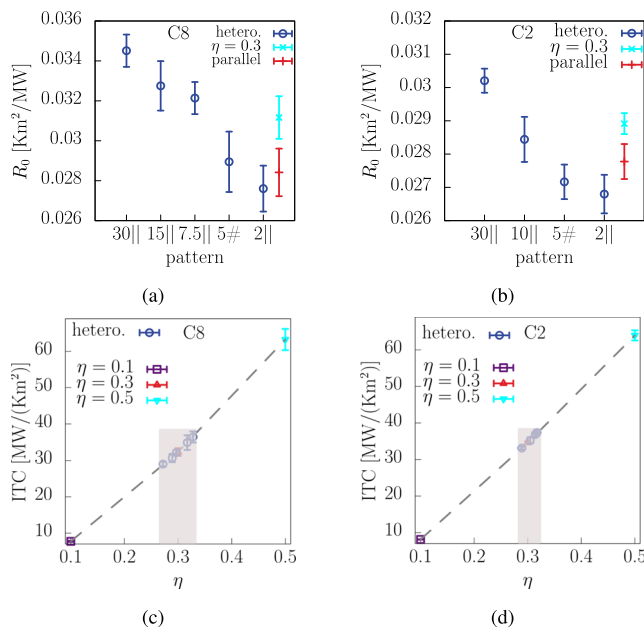


FIG. 10. (a) and (b) Comparisons among ITR of heterogeneous surface systems (blue), modeled ITR using the parallel model (red) and homogeneous surface system model with η of 0.3 (cyan). (c) and (d) ITC of homogeneous surface systems as a function of solid–liquid affinity, where the vertical gray shadow indicates the corresponding range of solid–liquid affinity of heterogeneous surface systems when mapping their ITC to homogeneous surface systems.

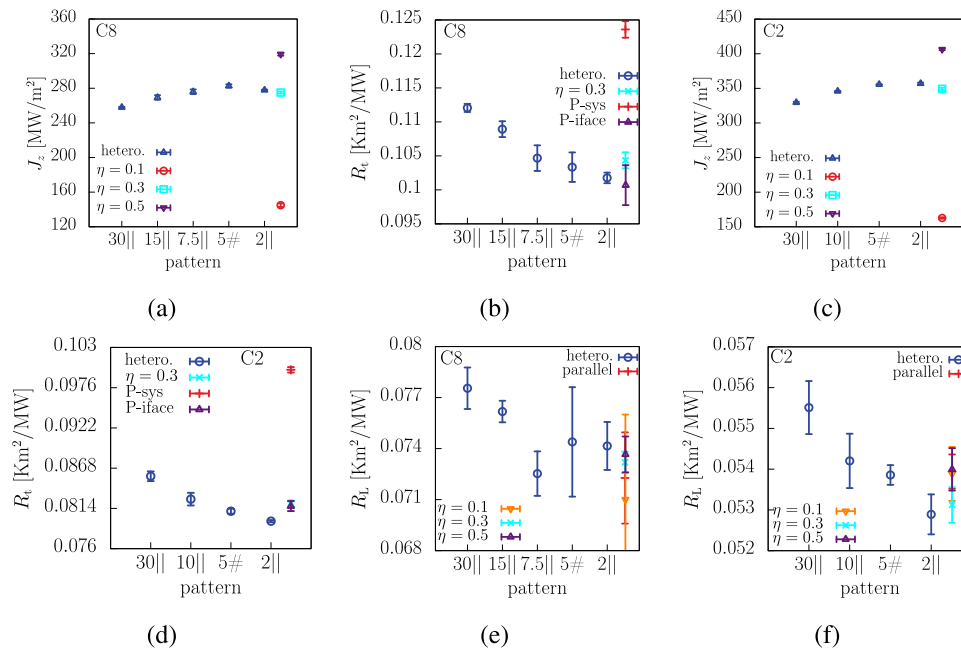


FIG. 11. (a)–(d) Heat flux of homogeneous and heterogeneous surface systems, and OTR comparisons among heterogeneous surface systems, modeled OTR using the parallel system model, parallel interface model, and homogeneous surface system model. (e) and (f) Comparisons of thermal resistance of liquid component.

of OTR should exhibit the same performance as the parallel system model of ITR. However, as shown in Figs. 11(e) and 11(f), the thermal resistance of liquid component (R_L) varies among different systems. This variability arises because R_L is still influenced by interfacial properties, as the temperature of the first liquid adsorption layer was used to calculate the temperature difference. The thermal resistance of the bulk part of the liquid can be identical under each system as illustrated in Fig. S10, despite the fact that we did not specifically investigate the segment of the liquid component that exhibits thermal conductivity independent of interfacial properties. As a result, the performance of the parallel interface model will mainly depend on the consistency of R_L among different systems since R_L is much larger than the ITR. Therefore, the function of the parallel interface model is similar to the homogeneous surface system model to roughly estimate the OTR of the heterogeneous surface system with a uniform or close to uniform temperature distribution.

In the macroscopic world, the parallel system model is effective for systems comprising solely solid components but exhibits limitations for systems containing both solid and liquid components due to the intricate energy and mass exchanges between the liquid components. It is the main reason why the parallel system approach fails to predict the OTR of heterogeneous surface systems at nanoscale. Fortunately, the parallel interface model does not require parallelizing liquid thermal resistance. It can be used as a rough estimation of the OTR of heterogeneous surface systems with a uniform temperature distribution. Accurately modeling the ITR and OTR of heterogeneous surface systems is challenging. The liquid should have a uniform distribution of properties near the solid–liquid interface, and the decomposed temperature jumps and heat fluxes should

be consistent with the corresponding homogeneous surface systems. At the nanoscale, even minor discrepancies can be amplified, making thermal resistance modeling more difficult.

IV. CONCLUSION

With the aid of molecular dynamics simulations, the size effects of chemical heterogeneity of solid–liquid polymer interfaces on interface thermal resistance (ITR) and overall thermal resistance (OTR) at the nanoscale were systematically investigated. The chemically heterogeneous substrate was comprised of alternating patches with weak and strong solid–liquid interfacial affinities. To characterize the heterogeneity size, we introduced the “affinity unevenness” parameter, which was defined as the ratio of the total length of the boundary between patches with different affinities to the surface area of the substrate. Our findings revealed a negative correlation between affinity unevenness and ITR, with OTR tendency being mainly determined by ITR. In particular, at the large heterogeneity size, i.e., large patch size, we observed a high degree of spatial unevenness in liquid adsorption sites on the substrate surface. This led to the large disparity between the interfacial heat flux contributed by strong solid–liquid interactions and that contributed by weak solid–liquid interactions, resulting in a non-uniform temperature distribution in the horizontal planes of liquid adsorption layers. The non-uniform temperature distribution increased ITR when compared to the homogeneous surface system with an intermediate solid–liquid affinity, which represented the average of weak and strong affinities. In contrast, a small chemical heterogeneity size

produced a uniform distribution of liquid adsorption sites on the solid surface. This enabled all liquid atoms in the adsorption layer to interact with high-affinity surface patches, resulting in a more uniform interfacial heat flux. A uniform distribution of interfacial properties is beneficial to enhance interfacial heat transfer. Therefore, the uniform distribution of temperature resulted in a reduction in ITR.

Existing research has demonstrated that the ITR of SLS systems can be effectively reduced by inducing polymer alignment in favorable directions. This motivated us to investigate if surface heterogeneity could be used to manipulate polymer orientation and thus ITR. Surprisingly, surface heterogeneity appeared to have no significant effect on polymer orientation, which was different from what we had observed for geometric heterogeneity. As a result, the ITR and OTR of chemically heterogeneous surface systems remained within the range observed in homogeneous surface systems. This range spans from those with a weak solid-liquid affinity to those with a strong affinity. Hence, we suggest primarily utilizing chemical heterogeneity to precisely control the ITR and OTR of SLS systems. In practical applications, when aiming for a slightly smaller ITR and OTR, it would be advantageous to graft $-COOH$ and $-CH_3$ terminated SAMs onto the substrate surface alternatively but tightly, and vice versa.

To provide a reference for the design of heterogeneous surfaces, we modeled the ITR and OTR using the data of homogeneous surface systems. The parallel electrical resistance analogy was successful in predicting the ITR of systems with small heterogeneity sizes whose temperature distributions were uniform. However, the influence of heat flux disparity between heterogeneous and homogeneous surface systems on OTR was amplified at the nanoscale. It led to the macroscopic model failing to predict OTR. Hence, we suggest simply using the liquid thermal resistance of homogeneous surface systems as an approximation of OTR of heterogeneous surface systems.

SUPPLEMENTARY MATERIAL

See the [supplementary material](#) for supporting content.

ACKNOWLEDGMENTS

Computational simulations were performed on the super-computer system “AFI-NITY” at the Advanced Fluid Information Research Center, Institute of Fluid Science, Tohoku University.

AUTHOR DECLARATIONS

Conflict of Interest

The authors have no conflicts to disclose.

Author Contributions

Qing-Yao Luo: Conceptualization (equal); Data curation (equal); Methodology (equal); Software (equal); Visualization (equal); Writing – original draft (equal); Writing – review & editing (equal). **Donatas Surblys:** Conceptualization (equal); Methodology (equal); Software (equal); Writing – review & editing (equal). **Hiroki Matsumura:** Conceptualization (equal); Methodology (equal); Writing –

review & editing (equal). **Taku Ohara:** Conceptualization (equal); Project administration (equal); Writing – review & editing (equal).

DATA AVAILABILITY

The data that support the findings of this study are available from the corresponding author upon reasonable request.

REFERENCES

- A. Giri and P. E. Hopkins, *Adv. Funct. Mater.* **30**, 1903857 (2020).
- J. Park, H. Jung, W. Kwon, G. Choi, J. Chang, and J. Jeon, *ACS Appl. Electron. Mater.* **5**, 2239 (2023).
- S. Wang, X. Liu, and P. Zhou, *Adv. Mater.* **34**, 2106886 (2022).
- A. K. Roy, B. L. Farmer, V. Varshney, S. Sihm, J. Lee, and S. Ganguli, *ACS Appl. Mater. Interfaces* **4**, 545 (2012).
- M. Shrivastava and V. Ramgopal Rao, *Nano Lett.* **21**, 6359 (2021).
- H. Huang, J. Hu, and H. Wang, *J. Semicond.* **35**, 084006 (2014).
- J. Long, Y. Li, Z. Ouyang, M. Xi, J. Wu, J. Lin, and X. Xie, *J. Colloid Interface Sci.* **628**, 534 (2022).
- M. Suttipong, B. P. Grady, and A. Striolo, *Phys. Chem. Chem. Phys.* **16**, 16388 (2014).
- P. Papadopoulos, X. Deng, L. Mammen, D.-M. Drotlef, G. Battagliarin, C. Li, K. Müllen, K. Landfester, A. Del Campo, H.-J. Butt, and D. Vollmer, *Langmuir* **28**, 8392 (2012).
- Y. Wen and Y. Liu, *Chem. Eng. Sci.* **258**, 117776 (2022).
- K. Gao, Y. Huang, Y. Han, Y. Gao, C. Dong, J. Liu, F. Li, and L. Zhang, *Macromolecules* **55**, 6620 (2022).
- J. A. Ritchie, J. S. Yazdi, D. Bratko, and A. Luzar, *J. Phys. Chem. C* **116**, 8634 (2012).
- J. Zhang, F. Müller-Plathe, and F. Leroy, *Langmuir* **31**, 7544 (2015).
- F.-C. Wang and H.-A. Wu, *Soft Matter* **9**, 5703 (2013).
- S. Gao, J. Qu, Z. Liu, and W. Liu, *Langmuir* **38**, 6352 (2022).
- X. Wei, T. Zhang, and T. Luo, *ACS Appl. Mater. Interfaces* **9**, 33740 (2017).
- Z. Liang and M. Hu, *J. Appl. Phys.* **123**, 191101 (2018).
- H. Bao, J. Chen, X. Gu, and B. Cao, *ES Energy Environ.* **1**, 16 (2018).
- Q.-Y. Luo, D. Surblys, H. Matsubara, and T. Ohara, “A molecular dynamics study on the solid-liquid polymer interface: insight into the effect of surface roughness scale and polymer chain length on interfacial thermal resistance,” *Mol. Phys.* e2321311 (published online, 2024).
- H. Pamuk and T. Halicioğlu, *Phys. Status Solidi A* **37**, 695 (1976).
- J. R. Errington and A. Z. Panagiotopoulos, *J. Phys. Chem. B* **103**, 6314 (1999).
- S. K. Nath, F. A. Escobedo, and J. J. de Pablo, *J. Chem. Phys.* **108**, 9905 (1998).
- J. L. Rivera, C. McCabe, and P. T. Cummings, *Phys. Rev. E* **67**, 011603 (2003).
- H. K. Chilukoti, G. Kikugawa, and T. Ohara, *Int. J. Heat Mass Transfer* **59**, 144 (2013).
- G. B. Sigal, M. Mrksich, and G. M. Whitesides, *J. Am. Chem. Soc.* **120**, 3464 (1998).
- P. J. O'Brien, S. Shenogin, J. Liu, P. K. Chow, D. Laurencin, P. H. Mutin, M. Yamaguchi, P. Keblinski, and G. Ramanath, *Nat. Mater.* **12**, 118 (2013).
- J. Di, Z. Yang, and Y. Duan, *AIP Adv.* **9**, 125105 (2019).
- X. Wu, J. Di, Z. Yang, and Y. Duan, *Langmuir* **38**, 8353 (2022).
- Y. Ueki, S. Matsuo, and M. Shibahara, *Int. Commun. Heat Mass Transfer* **137**, 106232 (2022).
- S. Plimpton, *J. Comput. Phys.* **117**, 1 (1995).
- X. Liu, D. Surblys, Y. Kawagoe, A. R. Bin Saleman, H. Matsubara, G. Kikugawa, and T. Ohara, *Int. J. Heat Mass Transfer* **147**, 118949 (2020).
- J. A. Izaguirre, D. P. Catarallo, J. M. Wozniak, and R. D. Skeel, *J. Chem. Phys.* **114**, 2090 (2001).
- B. Todd, D. J. Evans, and P. J. Davis, *Phys. Rev. E* **52**, 1627 (1995).
- D. Torii, T. Nakano, and T. Ohara, *J. Chem. Phys.* **128**, 044504 (2008).

- ³⁵Y. Jannot and A. Degiovanni, *Thermal Properties Measurement of Materials* (John Wiley & Sons, 2018), pp. 33–34.
- ³⁶G. F. Naterer, *Advanced Heat Transfer* (CRC Press, 2018), pp. 29–30.
- ³⁷H. Harikrishna, W. A. Ducker, and S. T. Huxtable, *Appl. Phys. Lett.* **102**, 251606 (2013).
- ³⁸D. Surblys, Y. Kawagoe, M. Shibahara, and T. Ohara, *J. Chem. Phys.* **150**, 114705 (2019).
- ³⁹T. Ohara, *J. Chem. Phys.* **111**, 9667 (1999).
- ⁴⁰D. Alexeev, J. Chen, J. H. Walther, K. P. Giapis, P. Angelikopoulos, and P. Koumoutsakos, *Nano Lett.* **15**, 5744 (2015).
- ⁴¹L. Shangchao and B. Markus J, “The effect of non-covalent functionalization on the thermal conductance of graphene/organic interfaces,” *Nanotechnol.* **24**(16), 165702 (2013).
- ⁴²Y. Kawagoe, D. Surblys, H. Matsubara, G. Kikugawa, and T. Ohara, *Langmuir* **36**, 6482 (2020).
- ⁴³A. A. Joshi, J. K. Whitmer, O. Guzmán, N. L. Abbott, and J. J. de Pablo, *Soft Matter* **10**, 882 (2014).
- ⁴⁴M. Zhang, M. He, H. Gu, A. Huang, and W. Xiang, *Ceram. Int.* **44**, 19319 (2018).
- ⁴⁵J. Chen, X. Xu, J. Zhou, and B. Li, *Rev. Mod. Phys.* **94**, 025002 (2022).